Electronic supplementary information

New insights on the spatial confinement mechanism of nucleation of biogenic aragonite crystals from bivalve nacre

Xin Feng*[a], Gangsheng Zhang[a]

Table S1 Summary of the nucleation sites of new tablets and controlling mechanisms during the growth of bivalve nacre in the literature

species	Nucleation sites of new tablets	Controlling mechanisms	References
Pinctada radiata, Mytilus exustus, Anomia simplex	Random sites	Not mentioned	Bevelander and Nakahara (1969)[1]
Pelecypods (i.e. bivalves)	Random sites	Not mentioned	Wise (1970)[2]
Mytilus edulis, Nueula suleata, Unio tumidus, Nautilus pompilius	On the margin of less soluble sectors of the underlying tablets	Not mentioned	Mutvei (1977)[3], Mutvei and Dunca (2010)[4]
Hyriopsis cumingii	The conjunction of the underlying tablets	Not mentioned	Xie et al. (2010)[5]
Pinctada margaritifera	Near and at the boundary between the underlying tablets	Alveolar matrix at the boundary between the underlying tablets	Rousseau et al. (2005)[6]
Pinctada margaritifera	Triple-junction of three underlying tablets	Acidic proteins at the triple-junction of three underlying tablets	Rousseau et al. (2009)[7]
Pinctada fucata	Near and at the boundary between two underlying tablets	Mineral bridges through the poles of the inerlamellar membranes (ILMs)	1972 Wada[8]
Theoretical modeling of the growth of the sheet nacre	Random positions	Mineral bridges through the poles of the ILMs	Coppersmith et al. (2009)[9]
Nucula sulcata	On the margin of the underlying tablets	Mineral bridges through the broken holes of the ILMs caused by the squeezing of underlying three approaching tablets	Checa et al. (2011)[10]

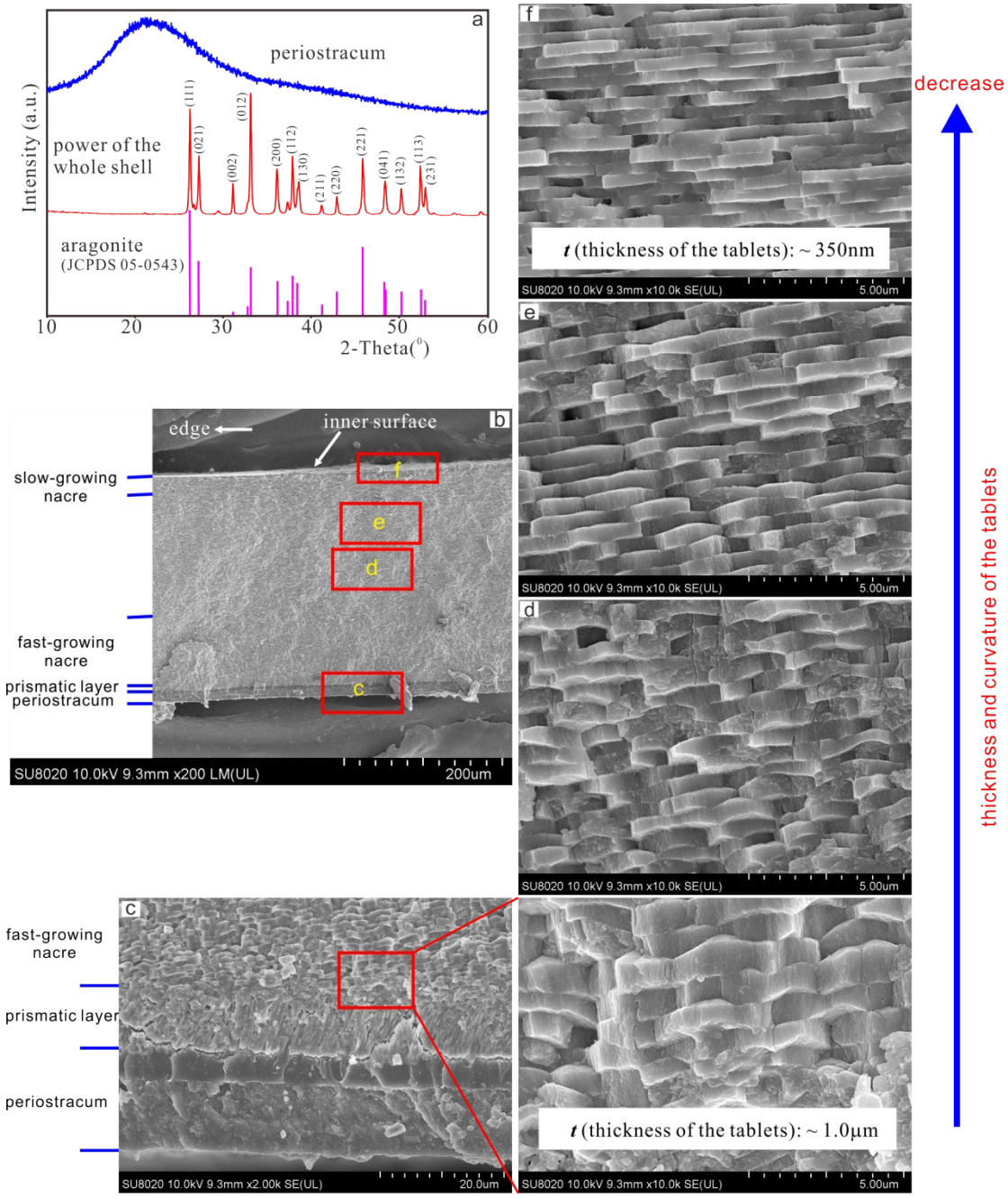

Fig. S1 X-ray diffraction (XRD) patterns of the powdered samples (a) and cross section (b) of the area 3 cut along the white line in Fig 1a. (c) – (f) correspond to the close up views of the boxed area c-f in (b). The shell length of this sample is 1.7cm (not the same shell as in Fig. 1a).

Please note that:

(1) The periostracum is amorphous, while the whole shell (including the prismatic layer and nacre) is of aragonite.

(2) The periostracum, prismatic layer, and nacre are about 16 μm, 9 μm, and 258 μm thick, respectively, in this sample, which usually increase with the shell size.

(3) Along the vertical direction, from the outer to the inner of the shell, the nacreous tablets vary gradually in thickness and curvature of their top surfaces, as detailed in our previous work[11]. Particularly, the slow-growing nacre exposed on the area 3 of the inner surface consists of flat tablets, which are similar to those of Mytilus edulis nacre.

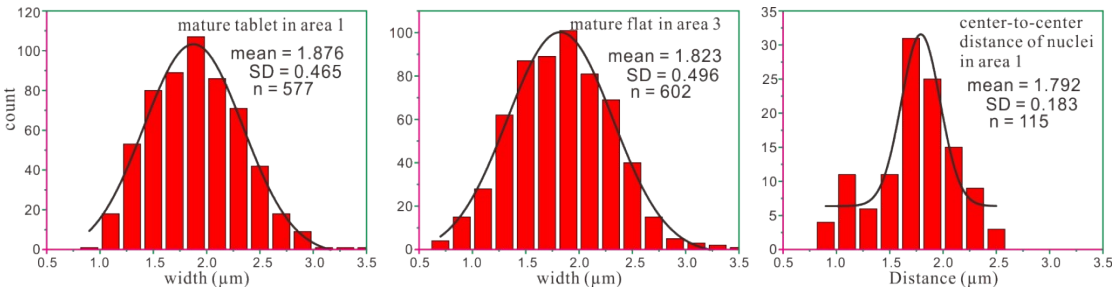

Fig. S2 Statistical histograms of the mature nacreous tablets size and center-to-center distance of nuclei.

Please note that:

(1) The mature nacreous tablets size and center-to-center distance of nuclei are not fixed, there is a certain range of fluctuations, namely the standard deviation;

(2) The size of mature nacreous tablets of *Perna virids* is small, the results are 1.876 ± 0.465 μ m (n = 577) (area 1), 1.823 ± 0.496 μ m(n = 602) (area 3), which consistent with the center-to-center distance of nuclei, namely 1.792±0.183 μ m (n = 115);

(3) When the distance of new nuclei is close, they will merge into one tablet in the growth process (circles in Fig. S3). Thus, the size of mature nacreous tablets still remains uniform.

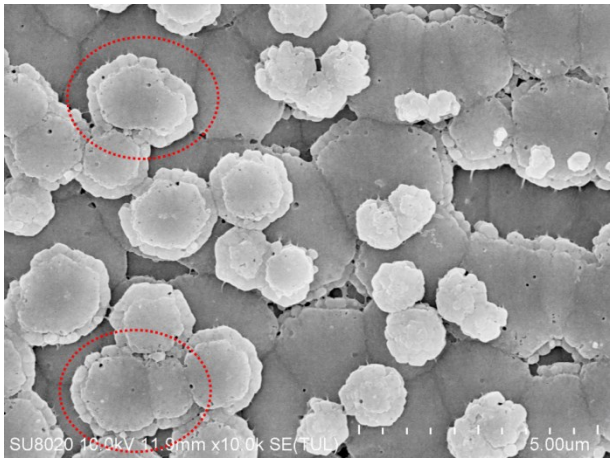

Fig. S3 Top view of SEM image showing two or several close tablets merge into one tablet (the circles). Samples sonicated in distilled water for 5 minute.

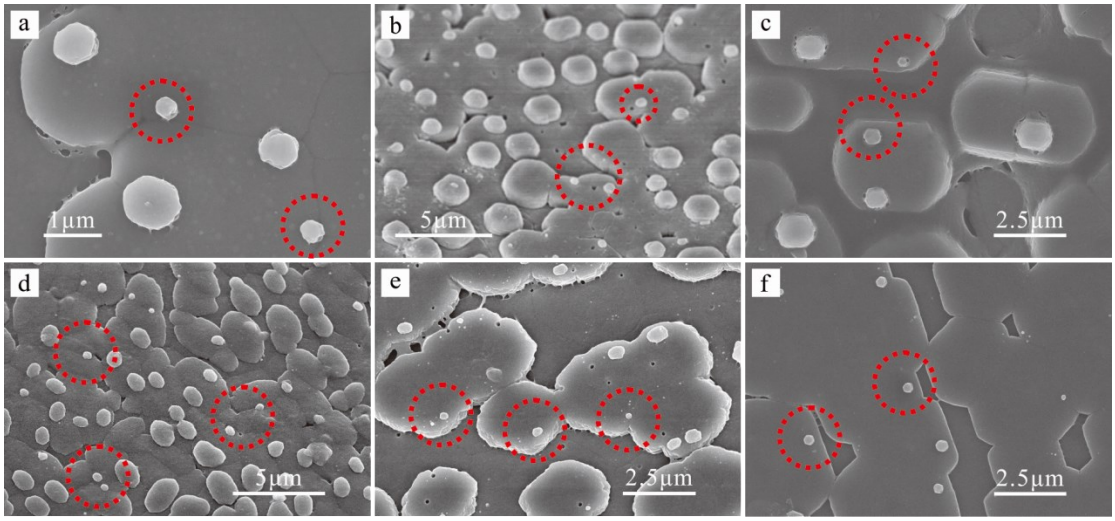

Fig. S4 Plan views of nacreous tablets of bivalves. (a) *Hyriopsis cumingii*; (b) *Mytilus coruscus*; (c) *Mytilus edulis*; (d) *Brachidontes setiger*; (e) *Modiolus kurilensis*; (f) *Pinctada martensi*.

Please note that:

In top views, the small new tablets (i.e. nuclei) are always nucleate on the margin of the underlying tablets: on the periphery of the isolated tablets (red circles in Fig. S4 b-c and e-f), close to the boundaries (Fig. S4 a: red circles), or close to the triple junction (Fig. S4 d: red circles).

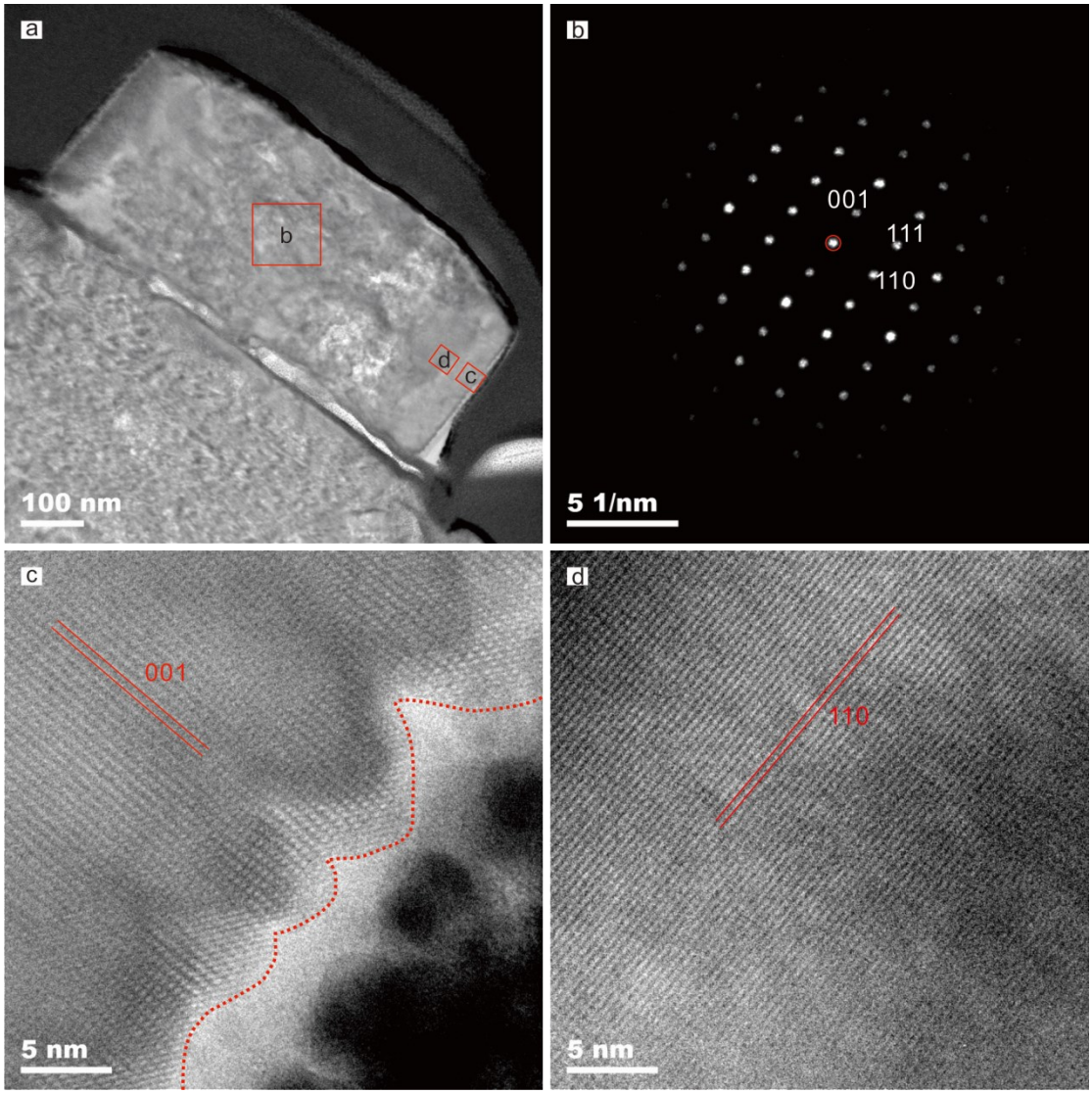

Fig. S5 (a) Bright-field TEM image of the vertical cross section prepared from ISS (area 3) by the FIB method. (b) SAED patterns of the boxed area b in (a). (c and d) HRTEM images of the boxed area c and d in (a), respectively.

Please note that:

The margin of the tablet is decorated with weakly crystalline nanoparticles (Fig. S5c: dashed lines). While close to center, the HRTEM image shows continuous lattice fringes of aragonite (110) (d=0.42nm) over the large area examined (Fig. S5d), which indicated the single crystal of aragonite, consistent with the SAED patterns (Fig. S5b), which show clear and regular diffraction spots of aragonite.

References：

1 G. Bevelander and H. Nakahara, *Calcif. Tissue Res.*, 1969, **3**, 84–92.

2 S. W. J. Wise, *Eclogae Geol. Helv.*, 1970, **63**, 775–797.

3 H. Mutvei, *Calcif. Tissue Res.*, 1977, **24**, 11–18.

4 H. Mutvei and E. Dunca, *Palaontologische Zeitschrift*, 2010, **84**, 457–465.

5 L. Xie, X. X. Wang and J. Li, *J. Struct. Biol.*, 2010, **169**, 89–94.

6 M. Rousseau, E. Lopez, A. Couté, G. Mascarel, D. C. Smith, R. Naslain and X. Bourrat, *J. Struct. Biol.*, 2005, **149**, 149–157.

7 M. Rousseau, A. Meibom, M. Gèze, X. Bourrat, M. Angellier and E. Lopez, *J. Struct. Biol.*, 2009, **165**, 190–195.

8 K. Wada, *Biomineralisation*, 1972, **6**, 141–159.

9 S. N. Coppersmith, P. U. P. A. Gilbert and R. A. Metzler, *J. Phys. A Math. Theor.*, 2009, **42**, 1–17.

10 A. G. Checa, J. H. E. Cartwright and M. G. Willinger, *J. Struct. Biol.*, 2011, **176**, 330–339.

11 J. Xu and G. Zhang, *Mater. Sci. Eng. C*, 2015, **52**, 186–193.